IN-20
19766
P17

NASA Technical Memorandum 104430
AIAA-91-2211

A Dual-Cooled Hydrogen-Oxygen Rocket Engine Heat Transfer Analysis

(NASA-TM-104430) A DUAL-COOLED HYDROGEN-OXYGEN ROCKET ENGINE HEAT TRANSFER ANALYSIS (NASA) 17 p CSCL 21H

N91-24302

Unclas
G3/20 0019766

Kenneth J. Kacynski, John M. Kazaroff,
and Robert S. Jankovsky
Lewis Research Center
Cleveland, Ohio

Prepared for the
27th Joint Propulsion Conference
cosponsored by the AIAA, SAE, ASME, and ASEE
Sacramento, California, June 24-27, 1991

NASA

A DUAL-COOLED HYDROGEN-OXYGEN ROCKET ENGINE

HEAT TRANSFER ANALYSIS

Kenneth J. Kacynski, John M. Kazaroff, and Robert S. Jankovsky

ABSTRACT

This report describes the potential benefits of simultaneously using hydrogen and oxygen as rocket engine coolants. A rocket engine was examined using a combined three-dimensional conduction/advection analysis. Both counter-flow and parallel flow cooling arrangements were analyzed. In all cases studied, hydrogen was the closest to the rocket engine combustion gasses and served as the primary coolant. The results indicate that a significant amount of heat transfer to the oxygen will occur, thereby, reducing both the hot side wall temperature of the rocket engine and also reducing the exit temperature of the hydrogen coolant.

At low heat flux/low coolant flow (i.e., throttled conditions), the oxygen coolant absorbed more than 30 percent of the overall heat transfer from the rocket engine combustion gasses. Also, hot side wall temperatures were predicted to decrease by approximately 120 K (200 °R) in the throat area and up to a 170 K (300 °R) combustion chamber wall temperature reduction is expected if dual cooling is applied. The reduction in combustion chamber wall temperatures at throttled conditions is especially desirable since the analysis indicates that a double temperature maxima, one at the throat and another in the combustion chamber, will occur with a traditional hydrogen cooled only engine.

INTRODUCTION

There has been considerable interest in space based liquid hydrogen-liquid oxygen propellant rocket engines, with specific emphasis towards lunar and interplanetary missions. In order to operate in such environments, these engines need to be highly efficient, reliable, reusable, and also be capable of multi-thrust levels of operation (i.e., throttlable).

The need for throttled engine mode operation places unique cooling demands on a rocket engine. Rocket chamber cooling at multi-thrust levels of operation can be especially difficult. Cooling designs are optimal only for a certain thrust level or chamber pressure condition, and may be inadequate at conditions far removed from this optimal design point. In general, operation at low thrust is limited because coolant temperatures become excessive, and operation at high thrust is limited because local heat fluxes become excessive.

Throttling also places difficulties on rocket engine injector performance. In general, injectors are also optimized for operation at very specific conditions, and operation at throttled, or "off-design" conditions, can be very difficult, due largely to decreased injection velocities.

It is possible that the operational limits of both the rocket engine nozzle and the injector can be extended by using both the oxygen and the hydrogen as rocket engine coolants (i.e., dual cooling). Used in this mode, the oxygen could theoretically reduce hydrogen coolant heat fluxes and temperatures, while at the same time serving as an oxygen preheater. In this paper, an analysis of the expectations and limitations of the dual cooling concept is performed.

BACKGROUND

Dual cooled hydrogen-oxygen rocket engines were designed and tested by Rockwell Corporation, in the early 1970's as part of the Air Force funded Aerospike Nozzle Program (ref. 1). The results of hot-fire testing indicated that the predicted heat transfer benefits of dual cooling could be experimentally verified. Unfortunately, manufacturing anomolies resulted in premature failure and extensive heat transfer measurements were not made.

From a manufacturing standpoint, the system studied herein offers significant improvement over the previously built aerospike nozzle. As the tubes used in the construction of the nozzle can be individually pressure tested before bonding together, leaks between the coolant chambers, such as experienced in the aerospike program, are very unlikely.

Furthermore, electroform buildup of the tube bundle/oxygen channel is a very consistent process, with the possibility of inadequate bonding substantially less than would be expected using a furnace braze technique. Consequently, it is the authors belief that the dual cooled system can, with some substantial manufacturing improvements, be used to both improve rocket engine performance and reliability.

MODEL DESCRIPTION

The rocket engine analyzed in this study was the plug-and-spool configuration (fig. 1) used extensively at NASA Lewis Research Center for chamber life testing. This configuration is well suited for life testing because the spool is easy to manufacture and its reduced size allows for low cost testing, but yet in conjunction with the plug allows for accurate duplication of failures which occur in a full size rocket. These failures are duplicated by creating sonic flow conditions in the exhaust gas (i.e., creating a throat region) with high heat fluxes. This high heat flux region is then used to test the relative lives of different materials and chamber coolant geometries. However, this type of engine in its standard 15.24 cm (6 in.) long configuration lacks the overall thermal characteristics of a full size engine to accurately illustrate the potential benefits of a dual cooled rocket engine. To better approximate the overall conditions of a full size chamber from the injector to nozzle attachment point, a 30.48 cm (12 in.) plug-and-spool engine was also analyzed.

Figure 2 shows a section of the chamber analyzed. Note the tubular hot gas side wall liner, which carries the hydrogen, and the channel oxygen heat exchanger. The configuration as shown was chosen for ease of test hardware fabrication.

PARAMETRIC STUDY

The perceived advantages of a dual-cooled rocket engine include increased engine life, performance, and throttlability. Engine life is often related to the maximum operating temperature of the cooling tube (ref. 2). Engine performance is related to the coolant tube pressure drop, as it degrades the potential operating pressure of the rocket engine. Coolant pressure drop, in turn is dependent on the cooling requirements of the fluid. For expander cycle engines, the inlet temperature of the hydrogen entering the turbines (after having exited the cooling jacket) also plays a significant role in engine performance. Engine throttling can be difficult for a variety of reasons. Two potentially limiting characteristics of throttling is that heat transfer rates to the coolant can become excessive and injector performance may often seriously degrade during a throttled operation.

Since rocket engine life, performance and throttling ability all depend on specific engine characteristics, the design engineer is forced to evaluate the merits of dual cooling on a case by case study. To examine the extent of the benefits available with dual cooling, a detailed, extensive, parametric study was performed at nominal rocket engine flowrates and chamber pressures, and at throttled conditions. Both parallel and counter flow coolant circuits are examined. The flow conditions analyzed are presented in table I.

The nominal condition considered for the plug-and-spool configuration is the operation of the rocket engine at 4100 kN/m^2 (600 psia) with 0.653 kg/sec (1.44 lb/sec) of hydrogen coolant flow, as described in reference 3. Axial variations in heat flux for the standard spool length case (using a smooth-walled configuration) have been measured (ref. 4) and are presented in figure 3. For the extended length spoolpiece analysis, the axial variation of heat transfer was assumed to have a similar profile. Heat flux profiles around the periphery of the tube (fig. 4) were assumed to have the profile calculated using a three-dimensional Navier-Stokes computational routine (ref. 5). This peripheral heat flux distribution was assumed to be independent of both axial location and chamber pressure.

Hydrogen flow rates and heat fluxes at conditions not previously tested at the NASA Lewis Research Center were assumed to scale with the nominal conditions in the following manner:

$$\frac{q''}{q''_{nom}} = \left\{\frac{m_{H_2}}{m_{H_{2_{nom}}}}\right\}^{0.8} \qquad (1)$$

The above relation can be obtained by assuming that the turbulent Ditteus-Boelter correlation (eq. (2)) is applicable and that the temperature difference between the hot gasses and the wall are insensitive to the heat flux. For the comparative purpose of this paper, the expression sufficiently models actual rocket scaling phenomena.

In the cases studied, the mixture ratio (O/F) was 6, and all available coolant was used (i.e., flow splitting was not considered).

Heat transfer analysis. - A three-dimensional conduction/advection analysis was performed to evaluate the dual-cooled rocket engine concept. The 1990 version of SINDA/FLUINT computer code (version 2.3A, ref. 6) was employed. The code is capable of performing a three-dimensional conduction analysis and "tieing" the analysis to a one-dimensional advection (heat and/or momentum transfer) calculation. Heat transfer and momentum exchange (via skin friction) from a solid wall to the fluid are calculated by employing the use of a heat transfer coefficient, h, and a friction factor, f, respectively. For the heat transfer coefficient calculation, the Ditteus-Boelter correlation (ref. 7) was used:

$$Nu = 0.023 Re^{0.8} Pr^{0.4} \qquad (2)$$

The smooth wall friction factor relation used was one proposed by Churchill to analytically represent the Moody chart (ref. 8):

$$f = 8\left(\left(\frac{8}{Re}\right)^{12} + \left(\frac{1}{(A+B)^{3/2}}\right)\right)^{1/12}$$

where

$$A = \left[-2.457\ln\left(\left(\frac{7}{Re}\right)^{0.9}\right)\right]^{16} \qquad (3)$$

$$B = \left(\frac{37530}{Re}\right)^{16}$$

Node and connector generation were obtained by using a PATRAN (ref. 8) preprocessing routine, PATSIN. Due to symmetry conditions, analysis of only one-half of one hydrogen coolant tube/oxygen coolant channel was sufficient to simulate a full 72 coolant tube/channelled configuration. The conduction elements (wherein the nodes correspond to the center of geometry) used for the dual flow analysis are shown in figure 5. As seen in the figure, 912 nodes were developed, with 12 axially varying and 76 circumferentially unique locations. Additionally, temperature nodes at all nonadiabatic surfaces were added to enhance solution accuracy.

Properties used in the fluid analysis correspond to conditions at 8200 kN/m^2 (1200 psi) for both the hydrogen and oxygen. The exception was that the density (which affect only pressure drop calculations) of the hydrogen was determined using the ideal gas law (i.e., $\rho = P/RT$). In the case of the oxygen coolant, incompressible fluid flow (density independent of fluid pressure) was assumed. An interpolating table of both fluid and material properties as a function of temperature were used in the analysis, as presented in table II.

Approximations to the axial and peripheral variation of heat flux were used as the measured (fig. 3) and calculated (fig. 4) heat flux distributions were more refined than was deemed necessary to screen the potential advantages of a dual cooled rocket engine. The numerical approximations, as shown in figures 6 and 7, were used as input conditions to the SINDA/FLUINT analysis, and were applied to all configurations examined. The heat flux profiles presented in these figures conserve total heat rates. However, wall temperature predictions at the throat may reflect a somewhat lower heat flux than would exist at nominal chamber pressure conditions because of the "smoothing" nature of the numerical approximations.

RESULTS AND DISCUSSIONS

In judging the potential for dual cooled rocket engines, several major heat transfer issues were considered. First, the total percentage of heat that is transferred to the oxygen circuit is an important parameter as it would relieve some of the coolant demands of the hydrogen circuit - a primary concern when operating at low chamber pressure conditions. Additionally, the total amount of heat transferred provides oxygen preheating, which could be used to improve injector performance. Chamber liner metal wall temperatures are also an important factor in evaluating the dual cooled concept. High throat temperatures and combustion chamber wall temperatures can be lowered by the dual cooling method. A summation of the more pertinent advantages follows. Complete results, including the axial variation of wall and coolant temperatures, is contained in the appendix.

Oxygen heat transfer abilities. - Oxygen coolant heat transfer abilities are presented in figure 8 for both the standard and the extended length spoolpiece simulations. From these results, it is apparent that the oxygen absorbs a substantial percentage of the total coolant heat transfer. At the lower heat fluxes, nearly 35 percent of the total coolant heat load is absorbed by the oxygen; the remainder going into the hydrogen. As flow rates increase, the resistance of the heat to transfer to the hydrogen decreases. Consequently, the amount of heat that transfers past the hydrogen tube and into the oxygen cooling circuit will decrease as coolant flow rates increase. This situation is borne out in figure 9, where the temperature distributions for the low coolant flow/low heat flux and the high coolant flow/high heat flux case are presented. In this figure, it is quite apparent that the driving potential for heat transfer from the copper substrate to the oxygen coolant, (i.e., temperature difference), is significantly lower in the high heat flux case, because the high velocity hydrogen coolant has suppressed wall temperatures. On the other hand, at the lowest heat transfer rates, temperature gradients within the copper are rather modest as most of the resistance to heat transfer is across the fluid. In this regime, the remoteness of the oxygen channel from the heat source is not a severe deterrent to heat transfer, and a more significant quantity of heat is carried out of the oxygen. Extending the length of the spoolpiece provides even more advantages of dual cooling. The higher oxygen cooling efficiency as combustor length increases is due to the fact that hydrogen temperatures increase faster than oxygen coolant temperatures, (due to a combination of mass flow, specific heat, and heat transfer efficiency calculations, as discussed in a later section). As a result, as the total amount of heating increases the driving potential for heat transfer becomes more skewed to transfer to the relatively colder fluid, the oxygen.

Oxygen coolant flow direction, whether parallel or counterflow, is seen to have very little overall effect on the oxygen coolant efficiency. This is somewhat counter to conventional intuition that counterflow heat exchangers performance is superior to parallel flow heat exchangers. However, for the cases analyzed in this study, results are primarily driven by the heat flux/coolant flow rate conditions previously described, and the temperature difference between the coolants had only a secondary effect, as described in the previous paragraph.

Oxygen preheating. - An important factor concerning injector performance when throttling at low mass flow rates is the maintenance of injection velocities, and injector pressure drops in order to avoid feed system flow instabilities (chugging). One way of accomplishing this is to cause the density of the propellants to decrease as the flow rate is decreased. Heating both propellants provides a significant decrease in density of the oxygen propellant. For the throttled simulation studied, the density of the oxygen decreased by a factor of 4. Therefore, the potential for improved injector performance is possible.

Hot side throat wall temperature. - In many instances, rocket nozzle cooling is most difficult at the throat, where local heat fluxes are greatest. Figure 10 presents the effect that dual cooling has towards reducing wall throat temperatures for the extended length simulation. Several things regarding dual cooling are apparent. First, wall temperatures are decreased very modestly (17 K (30 °R)) at high rocket engine heat fluxes. On the other hand, at the low heat flux simulation, the wall temperatures decreased by more than 120 K (220 °R) because of dual cooling.

Again, the improved abilities of the oxygen to extract heat at lower heat fluxes, as described previously, also results in increased capability of reducing wall temperatures at the throttled conditions.

Hot side combustor wall temperatures. - In expander cycle rocket engine operating environments, combustion chambers can become difficult to cool as the hydrogen temperatures are heated to their maximum possible temperature in order to operate turbomachinery most efficiently. Further, at throttled conditions, the difficulties of coolant overheating can become acute as the ratio of coolant flow rate/total heat transfer increases as the engine is throttled (eq. (1)).

The numerically simulated case of the throttled, extended length spoolpiece rocket combustor is shown in figure 11. In this situation, a double wall temperature maxima, one at the throat and another in the combustion chamber, exists when conventional cooling is used. The existence of this double maxima occurs because the hydrogen is being warmed to a temperature where its ability to act as a coolant is becoming marginal. However, with dual cooling, combustion chamber wall temperatures decrease significantly, especially with the counter flow cooling arrangements where the maximum chamber temperature reduction is over 170 K (300 °R).

SUMMARY OF RESULTS

The results of the dual-cooled spoolpiece rocket engine numerical simulation indicate that:

1. Dual cooling is extremely effective at low heat flux levels. At the 4100 kN/m^2, (75 psia) chamber pressure simulation, nearly 35 percent of the total heat transfer from the rocket exhaust gases was transferred to the oxygen. Further, wall temperatures at the throat and at the combustion chamber were reduced by over 200 °F. Finally, improved injector performance by means of oxygen preheating is possible as the oxygen density decreased by a factor of four, due solely to the thermal heating of the oxygen coolant.

2. At high heat flux/high coolant flow conditions, dual cooling effectiveness is modest, as throat temperatures were reduced by 17 K (30 °R). This modest benefit occurs because of the large hydrogen coolant flow rate and the design of the dual cooled system, as the heat from the exhaust gases traveled mostly into the hydrogen, with little heat transferring along the hydrogen cooled tube and into the oxygen cooling channel. Using a more oxygen heat transfer conducive design, the magnitude of the wall temperature reduction could be improved, however the general trend of reduced oxygen heat transfer efficiency with increasing coolant flow rates will remain.

3. The flow direction of the oxygen cooling circuit had little effect on heat transfer efficiencies. This is the result of the difference in coolant fluid temperatures, in general, being much less than the temperature difference between the wall and the coolant.

CONCLUDING REMARKS

A novel means of potentially expanding the window of operation of liquid hydrogen/liquid oxygen rocket engines, by using both the hydrogen and the oxygen as coolants, has been identified and simulated with a plug-and-spoolpiece rocket engine. The results indicate that by using oxygen and hydrogen as coolants, significant benefits can be realized for the hydrogen tube/oxygen channel spoolpiece configuration that was analyzed. The concept analysis should be applied towards an actual flight-designed rocket engine with total system interaction effects taken into account. Experimentation is also necessary to verify the numerically simulated advantages of dual cooling.

APPENDIX

A complete listing of the predicted axial distribution of the hot side wall temperature, and fluid temperatures are tabulated in tables III to V for all heat transfer, coolant flow directions, and spoolpiece lengths analyzed.

REFERENCES

1. Moses, D., Cordill, J., Shoji, J., Munyon, W., "O_2/H_2 Advanced maneuvering Propoulsion Technology Program," AFRPL-TR-76-05.

2. Jankovsky, R.S., and Kazaroff,J.M., "A Life Comparison of Tube and Channel Cooling Passages for Thrust Chambers," NASA TM 103613, 1990.

3. Quentmeyer, R.J., "Experimental Fatigue Life Investigation of Cylindrical Thrust Chambers," NASA TM 103613, 1990.

4. Roncace, E.A. and Quentmeyer, R.J., "Hot-gas-side Heat Transfer Characteristics of a Subscale Plug-Nozzle Rocket Chamber," To be published 1991.

5. Kacynski, K.J., "A Three-Dimensional Turbulent Heat Transfer Analysis for Advanced Tubular Rocket Thrust Chambers," NASA TM-103293, 1990.

6. SINDA 1985/FLUINT V.2.3, Martin Marietta Corporation, Denver Aerospace, NASA contract NAS9-17448.

7. Dittus, F.W., and Boelter, L.M.K., Univ. Calif., Berkely, Publ. Eng., Vol. 2, 1930, p. 443.

8. Moody, L.F., Trans. ASME, Vol. 66, p. 671, 1944.

9. PATRAN Users Guide, PDA Engineering Software Products Division, Santa Ana, CA., 1985.

TABLE I. - FLOW RATE & HEAT FLUX PARAMETERS EXAMINED

	Low pressure		Nominal conditions		High pressure	
Spool length, cm (in.)	15.24 (6)	30.48 (12)	15.24 (6)	30.48 (12)	15.24 (6)	30.48 (12)
Chamber pressure,* kN/m^2 (psia)	520 (75)	520 (75)	4100 (600)	4100 (600)	19000 (2700)	19000 (2700)
Throat crown heat flux, MW/m^2 (Btu/in.^{2} sec)	9.29 (5.68)	9.29 (5.68)	49.0 (30)	49.0 (30)	163.5 (100)	163.5 (100)
Hydrogen flow rate, kg/s (lb/sec)	.0816 (.180)	.0816 (.180)	.653 (1.44)	.653 (1.44)	2.94 (6.48)	2.94 (6.48)
Oxygen flow rate, kg/s (lb/sec)	.490 (1.08)	.490 (1.08)	3.92 (8.64)	3.927 (8.64)	17.64 (38.88)	17.64 (38.88)
Total heat transfer to coolant, MW (Btu)	1.758 (1666)	3.514 (3331)	9.281 (8797)	18.562 (17594)	30.937 (29324)	61.873 (58647)

*Approximate, not directly used in dual cooled analysis.

TABLE II. - PROPERTIES USED FOR DUAL COOLED ANALYSIS

(a) Copper thermal conductivity.

T, K	T, (°R)	k, W/m K	k, (Btu/ft hr °R)
0		451.5	(260.5)
200	(360)	413.2	(238.4)
400	(720)	393.2	(227.2)
600	(1080)	379.0	(219.0)
800	(1440)	352.0	(203.4)
1000	(1800)	352.0	(203.4)
1200	(3160)	338.9	(195.8)

(b) Hydrogen properties.

T, K	T, (°R)	Cp, kJ/kg K	Cp, (Btu/lb_m °R)	k, W/m K	k, (Btu/ft hr °R)	$\mu \times 10^3$, kN s/m^2	$\mu \times 10^3$, (lb_m/ft hr)
16.3	(29.4)	6.539	(1.562)	.0113	(.05853)	3.0641	(7.4124)
22.2	(40)	8.532	(2.038)	.1237	(.07147)	1.8020	(4.3596)
33.3	(60)	12.183	(2.91)	.1242	(.07175)	1.0298	(2.4912)
52.8	(95)	17.265	(4.124)	.09304	(.05376)	.5610	(1.3572)
88.9	(160)	15.172	(3.624)	.09188	(.05309)	.4792	(1.1592)
177.8	(320)	16.943	(4.047)	.15807	(.09134)	.6741	(1.6308)
288.9	(520)	15 151	(3.619)	.1780	(.10286)	.8170	(1.9764)
388.9	(700)	14 737	(3.52)	.2000	(.11556)	.9385	(2.268)

(c) Oxygen properties.

T, K	T, (°R)	Cp, kJ/kg K	Cp, (Btu/lb_m °R)	k, W/m K	k, (Btu/ft hr °R)	$\mu \times 10^6$, kN s/m^2	$\mu \times 10^6$, (lb_m/ft hr)	ρ, kg/m^3	ρ, (lb_m/ft^3)
55.3	(100)	1.658	(.396)	.1944	(.1123)	64.47	(155.95)	1312	(81.9)
77.8	(140)	1.6543	(.395)	.1713	(.0990)	31.08	(75.168)	1215	(75.8)
105.6	(190)	1.6963	(.405)	.1372	(.0795)	14.68	(35.507)	1085	(67.7)
133.3	(240)	1.9263	(.460)	.1010	(.0584)	8.651	(20.927)	926	(57.8)
161.1	(290)	3.6133	(.863)	.0657	(.0380)	5.153	(12.467)	647	(40.4)
211.1	(380)	1.4403	(.344)	.0318	(.0184)	2.415	(5.843)	191	(11.9)
266.7	(480)	1.1093	(.265)	.0316	(.0183)	2.473	(5.983)	129	(8.1)

TABLE III. - THROTTLED ENGINE SIMULATION
($P_c \simeq 520 kN/m^2$ (75 psi))

Predicted Temperatures, K (°R)

x/L*	No oxygen channel: H_2, K	($°R$)	No oxygen channel: Wall***, K	($°R$)	Counter-flow oxygen: H_2, K	($°R$)	Counter-flow oxygen: O_2, K	($°R$)	Counter-flow oxygen: Wall***, K	($°R$)	Parallel-flow oxygen: H_2, K	($°R$)	Parallel-flow oxygen: O_2, K	($°R$)	Parallel-flow oxygen: Wall***, K	($°R$)
STANDARD LENGTH																
0	44.4	(80.0)			44.4	(80.0)	203.9	(367.1)			44.4	(80.0)	90.0	(162.0)		
.0833	48.3	(86.9)	110.3	(198.6)	49.3	(88.7)	208.2	(374.8)	115.2	(207.4)	47.6	(85.7)	90.3	(162.5)	99.8	(179.6)
.1667	53.7	(96.6)	139.6	(251.3)	54.4	(97.9)	211.7	(381.1)	127.8	(230.0)	51.4	(92.6)	91.5	(164.7)	115.4	(207.7)
.2500	67.4	(121.3)	305.1	(549.2)	65.7	(118.2)	208.7	(375.7)	244.5	(440.1)	61.3	(110.4)	97.7	(175.8)	244.9	(440.8)
.3333**	91.2	(164.2)	483.7	(870.7)	84.0	(151.2)	198.8	(357.8)	372.6	(670.7)	78.2	(140.7)	109.3	(196.7)	386.7	(696.0)
.4167	116.9	(210.4)	499.3	(898.7)	103.2	(185.7)	186.2	(335.2)	380.8	(685.5)	96.2	(173.2)	121.0	(217.8)	400.5	(720.9)
.5000	138.3	(249.0)	448.4	(807.1)	118.9	(214.0)	174.6	(314.2)	340.7	(613.2)	111.4	(200.6)	130.4	(234.7)	355.9	(642.5)
.5833	155.5	(279.9)	399.1	(718.4)	131.1	(236.0)	164.1	(295.4)	302.3	(544.1)	123.5	(222.3)	137.6	(247.6)	315.0	(567.0)
.6667	170.3	(306.6)	378.9	(682.1)	141.4	(254.6)	153.3	(275.9)	285.5	(515.7)	133.9	(241.0)	142.9	(257.3)	298.3	(537.0)
.7500	183.4	(330.2)	370.3	(666.6)	150.5	(270.9)	139.0	(250.2)	278.3	(500.9)	143.2	(257.7)	147.4	(265.4)	290.5	(522.9)
.8333	193.8	(348.9)	342.0	(615.6)	157.1	(282.8)	120.6	(217.0)	253.4	(456.1)	150.4	(270.8)	193.9	(271.4)	266.7	(478.3)
.9167	199.6	(359.2)	278.1	(500.6)	159.7	(285.5)	104.8	(188.6)	199.9	(359.9)	154.1	(277.4)	152.6	(274.6)	211.2	(380.1)
1.000	202.8	(365.0)	246.4	(443.6)	160.4	(288.7)	90.0	(162.0)	174.1	(313.3)	156.1	(280.9)	153.6	(276.4)	185.6	(334.1)
EXTENDED LENGTH																
0	44.4	(80.0)			44.4	(80.0)	203.9	(367.1)			44.4	(80.0)	90.0	(162.0)		
.0833	50.2	(90.4)	98.2	(176.8)	54.8	(98.6)	208.2	(374.8)	135.1	(243.1)	50.0	(90.0)	90.1	(162.1)	96.4	(173.6)
.1667	57.4	(103.3)	117.6	(211.7)	65.2	(117.4)	211.7	(381.1)	148.6	(267.4)	55.8	(100.4)	91.2	(164.1)	105.4	(189.8)
.2500	85.5	(153.9)	319.9	(575.9)	90.7	(163.3)	208.7	(375.7)	301.4	(542.5)	75.4	(135.7)	104.2	(187.5)	253.7	(456.7)
.3333**	138.5	(249.3)	515.2	(929.2)	132.9	(239.2)	198.8	(357.8)	452.1	(813.7)	112.3	(202.2)	128.3	(230.9)	412.0	(741.6)
.4167	188.9	(340.0)	542.7	(976.8)	170.9	(307.6)	186.2	(335.2)	454.7	(818.4)	147.1	(264.8)	148.3	(266.9)	418.8	(753.8)
.5000	230.7	(415.2)	525.2	(945.3)	198.7	(357.6)	174.6	(314.2)	414.9	(746.8)	173.8	(312.9)	160.5	(288.9)	381.5	(686.7)
.5833	265.4	(477.7)	503.6	(906.5)	218.6	(393.5)	164.1	(295.4)	376.8	(678.3)	194.3	(349.8)	169.8	(305.7)	356.6	(641.9)
.6667	297.3	(535.1)	511.0	(919.8)	234.4	(421.9)	153.3	(275.9)	363.2	(653.7)	212.7	(382.8)	179.2	(322.6)	357.1	(642.8)
.7500	327.2	(589.0)	525.6	(946.0)	247.7	(445.9)	139.0	(250.2)	359.9	(647.8)	230.1	(414.1)	188.8	(339.9)	365.8	(658.4)
.8333	351.4	(632.5)	510.0	(918.0)	256.8	(462.2)	120.6	(217.0)	337.8	(608.1)	244.1	(439.3)	197.3	(355.2)	352.5	(634.5)
.9167	363.2	(653.8)	439.7	(791.4)	257.1	(462.8)	104.8	(188.6)	278.7	(492.6)	249.7	(449.5)	202.5	(364.5)	295.6	(532.1)
1.000	369.2	(664.5)	407.6	(733.7)	253.3	(455.9)	240.4	(162.0)	240.4	(432.8)	251.7	(453.1)	205.9	(370.7)	269.8	(485.6)

* As measured from hydrogen inlet (see fig. 1).

** Throat location

*** Wall Temperatures correspond to point midway between stated and preceding axial location.

TABLE IV. - BASELINE ENGINE SIMULAITON
($P_c \simeq 4100 kN/m^2$ (600 psi))

Predicted Temperatures, K (°R)

STANDARD LENGTH									
	NO OXYGEN CHANNEL		COUNTER-FLOW OXYGEN			PARALLEL-FLOW OXYGEN			
x/L*	H_2	Wall***	H_2	O_2	Wall***	H_2	O_2	Wall***	
0	44.4 (80.0)		44.4 (80.0)	116.7 (210.0)		44.4 (80.0)	90.0 (162.0)		
.0833	46.4 (83.5)	110.3 (198.5)	46.8 (84.2)	117.3 (211.2)	110.7 (199.2)	46.4 (83.5)	89.9 (161.9)	110.9 (199.7)	
.1667	48.6 (87.5)	120.2 (216.4)	49.2 (88.6)	117.8 (212.1)	115.3 (207.6)	48.4 (87.2)	90.0 (162.0)	116.3 (209.4)	
.2500	57.6 (103.6)	381.6 (686.8)	57.2 (102.9)	116.3 (209.4)	336.3 (605.3)	56.0 (100.8)	92.4 (166.3)	355.1 (639.1)	
.3333**	74.3 (133.7)	679.0 (1222.2)	71.4 (128.6)	112.4 (202.4)	587.1 (1056.7)	69.7 (125.4)	97.3 (175.1)	626.1 (1127.0)	
.4167	92.0 (165.6)	687.0 (1236.6)	86.1 (155.0)	108.1 (194.6)	592.4 (1066.4)	83.8 (150.8)	102.4 (184.4)	631.2 (1136.1)	
.5000	106.7 (192.1)	576.0 (1036.8)	98.5 (177.3)	104.4 (188.0)	500.4 (900.8)	95.8 (172.4)	106.7 (192.1)	533.0 (959.4)	
.5833	118.3 (213.0)	481.1 (866.0)	108.1 (194.5)	101.3 (182.3)	418.6 (753.5)	105.2 (189.3)	110.1 (198.1)	443.9 (799.1)	
.6667	128.5 (231.3)	445.4 (801.8)	116.4 (209.6)	98.4 (177.1)	388.1 (698.5)	113.5 (204.3)	113.1 (203.5)	410.4 (738.7)	
.7500	137.8 (248.1)	429.4 (773.0)	124.2 (223.5)	95.5 (171.9)	374.4 (674.0)	121.2 (218.1)	115.8 (208.5)	395.2 (711.4)	
.8333	145.3 (261.5)	377.5 (679.5)	130.2 (234.3)	93.0 (167.4)	328.8 (591.9)	127.3 (229.1)	118.1 (212.6)	345.7 (622.2)	
.9167	148.9 (268.0)	257.4 (463.3)	132.7 (238.9)	91.3 (164.3)	221.4 (398.6)	130.1 (234.1)	119.3 (214.8)	230.1 (414.1)	
1.000	150.7 (271.3)	205.3 (369.6)	133.7 (240.7)	90.0 (162.0)	175.1 (315.2)	131.4 (236.5)	120.1 (216.2)	180.4 (324.7)	
0	44.4 (80.0)		44.4 (80.0)	150.0 (270.0)		44.4 (80.0)	90.0 (162.0)		
.0833	48.1 (86.6)	110.1 (198.2)	49.7 (89.5)	151.4 (272.5)	124.8 (224.7)	48.3 (86.9)	89.8 (161.7)	111.4 (200.6)	
.1667	51.8 (93.3)	114.8 (206.6)	54.7 (98.4)	152.7 (274.8)	128.4 (231.1)	51.9 (93.4)	89.8 (161.7)	114.1 (205.3)	
.2500	69.9 (125.8)	393.2 (707.8)	70.7 (127.2)	150.7 (271.3)	375.8 (676.4)	66.8 (120.2)	94.9 (170.8)	364.1 (655.4)	
.3333**	106.0 (190.8)	694.2 (1249.6)	100.4 (180.8)	144.9 (260.8)	647.4 (1165.4)	95.8 (172.4)	105.6 (190.1)	643.8 (1158.8)	
.4167	141.1 (254.0)	684.6 (1232.2)	129.3 (232.7)	138.0 (248.4)	638.6 (1149.4)	124.6 (224.2)	115.8 (208.4)	635.8 (1144.5)	
.5000	168.6 (303.5)	591.1 (1063.9)	151.8 (273.2)	130.8 (235.5)	548.6 (987.4)	147.0 (264.6)	124.1 (223.3)	545.8 (982.4)	
.5833	190.0 (342.0)	520.7 (937.3)	168.7 (303.6)	123.9 (223.1)	471.9 (849.4)	164.1 (295.4)	130.8 (235.4)	469.6 (845.2)	
.6667	210.5 (378.9)	506.7 (912.0)	183.1 (329.5)	116.8 (210.3)	448.1 (806.5)	178.8 (321.9)	136.8 (246.3)	445.3 (801.6)	
.7500	227.9 (410.2)	509.0 (916.2)	196.1 (353.0)	109.1 (196.3)	442.8 (797.1)	192.3 (346.2)	142.2 (255.9)	441.6 (794.9)	
.8333	243.2 (437.7)	471.8 (849.3)	206.1 (370.9)	101.3 (182.4)	401.7 (723.0)	202.9 (365.2)	146.4 (263.6)	402.6 (724.6)	
.9167	250.3 (450.6)	356.1 (641.0)	209.2 (376.6)	95.3 (171.5)	290.3 (522.5)	207.0 (372.6)	149.2 (268.5)	293.6 (528.5)	
1.000	254.0 (457.2)	306.8 (552.3)	209.5 (377.1)	90.0 (162.0)	241.6 (434.9)	208.3 (374.9)	151.2 (272.1)	246.9 (444.5)	

* As measured from hydrogen inlet (see fig. 1).
** Throat location
*** Wall Temperatures correspond to point midway between stated and preceding axial location.

TABLE V. - HIGH HEAT FLUX ENGINE SIMULATION
($P_c \simeq 19000 kN/m^2$ (2600 psi))

Predicted Temperatures, K (°R)

	NO OXYGEN CHANNEL				COUNTER-FLOW OXYGEN						PARALLEL-FLOW OXYGEN					
x/L*	H_2		Wall***		H_2		O_2		Wall***		H_2		O_2		Wall***	
STANDARD LENGTH																
0	44.4	(80.0)			44.4	(80.0)	102.5	(184.5)			44.4	(80.0)	90.0	(162.0)		
.0833	45.8	(82.5)	142.7	(256.8)	46.0	(82.8)	102.4	(184.5)	137.6	(247.6)	45.9	(82.6)	90.5	(162.9)	143.9	(259.0)
.1667	47.3	(85.1)	146.6	(263.9)	47.6	(85.6)	102.4	(184.3)	140.3	(252.5)	47.4	(85.3)	90.7	(163.2)	147.0	(264.6)
.2500	54.0	(97.2)	567.5	(1021.5)	54.0	(97.2)	101.6	(182.8)	525.5	(945.9)	53.7	(96.6)	91.7	(165.1)	560.4	(1008.7)
.3333**	66.4	(119.5)	1062.4	(1912.4)	65.6	(113.0)	99.9	(179.8)	978.1	(1760.5)	65.1	(117.1)	93.7	(168.6)	046.4	(1883.6)
.4167	79.2	(142.5)	1060.2	(1908.4)	77.4	(139.3)	98.2	(176.7)	975.1	(1755.2)	76.7	(138.0)	95.7	(172.3)	042.3	(1876.1)
.5000	90.1	(162.1)	878.6	(1581.4)	87.3	(157.2)	96.6	(173.9)	807.7	(1453.9)	86.5	(155.7)	97.4	(175.4)	862.9	(1553.3)
.5833	98.8	(177.8)	703.6	(1266.5)	95.4	(171.7)	95.2	(171.4)	650.9	(1171.7)	94.4	(170.0)	98.9	(178.1)	693.3	(1247.9)
.6667	106.4	(191.6)	637.4	(1147.3)	102.5	(184.5)	93.9	(169.1)	591.2	(1064.1)	101.4	(182.6)	100.3	(180.6)	627.7	(1129.8)
.7500	113.6	(204.5)	606.0	(1090.8)	109.1	(196.3)	92.7	(166.9)	565.8	(1013.00	108.0	(194.4)	101.7	(183.1)	599.7	(1079.4)
.8333	119.4	(214.9)	513.1	(923.6)	114.3	(205.8)	91.6	(164.8)	477.2	(858.9)	113.2	(203.8)	102.9	(185.2)	503.7	(906.7)
.9167	122.1	(219.7)	301.2	(542.2)	116.7	(210.0)	90.7	(163.3)	280.8	(505.4)	115.6	(208.1)	103.7	(186.6)	292.6	(526.7)
1.000	123.4	(222.2)	212.3	(382.2)	117.8	(212.0)	90.0	(162.0)	198.3	(357.0)	116.7	(210.2)	104.3	(187.8)	204.1	(367.3)
EXTENDED LENGTH																
0	44.4	(80.0)			44.4	(80.0)	121.4	(218.6)			44.4	(80.0)	90.0	(162.0)		
.0833	47.2	(84.9)	143.1	(257.6)	47.7	(85.8)	121.6	(218.8)	147.1	(264.7)	47.3	(85.2)	90.9	(163.7)	142.2	(256.0)
.1667	49.8	(89.7)	145.1	(261.2)	50.8	(91.4)	121.6	(218.8)	148.6	(267.5)	50.1	(90.2)	91.3	(164.4)	146.1	(262.9)
.2500	63.1	(113.5)	576.7	(1038.0)	63.3	(113.9)	119.8	(215.6)	571.4	(1028.6)	62.4	(112.3)	93.6	(168.4)	568.7	(1023.7)
.3333**	89.4	(160.9)	1087.2	(1957.0)	87.4	(157.3)	115.9	(208.7)	1071.0	(1927.8)	86.2	(155.2)	97.8	(176.0)	068.7	(1923.7)
.4167	116.1	(209.0)	1054.3	(1897.7)	111.9	(201.4)	111.0	(201.4)	1041.8	(1875.3)	110.6	(199.1)	102.1	(183.8)	041.7	(1875.0)
.5000	137.2	(247.0)	870.6	(1567.0)	131.1	(236.0)	108.2	(194.8)	858.3	(1544.9)	129.8	(233.7)	105.9	(190.7)	857.8	(1544.1)
.5833	153.5	(276.3)	713.9	(1285.1)	145.8	(262.5)	104.9	(188.8)	701.3	(1262.4)	144.6	(260.3)	109.3	(196.7)	701.0	(1261.8)
.6667	167.9	(302.2)	658.9	(1186.0)	158.6	(285.4)	101.5	(182.7)	645.2	(1161.4)	157.4	(283.4)	112.6	(202.6)	645.1	(1161.1)
.7500	181.2	(326.1)	638.2	(1148.7)	170.2	(306.4)	98.0	(176.4)	621.1	(1118.0)	169.3	(304.7)	115.8	(208.4)	621.2	(1118.2)
.8333	191.9	(345.5)	562.3	(1012.1)	179.4	(322.9)	94.7	(170.4)	539.9	(971.8)	178.6	(321.5)	118.8	(213.8)	539.9	(971.9)
.9167	197.0	(354.6)	365.9	(658.6)	183.1	(329.5)	91.9	(165.4)	344.7	(620.5)	182.5	(328.5)	121.1	(218.0)	345.3	(621.6)
1.000	199.6	(359.2)	283.5	(510.3)	183.4	(331.9)	90.0	(162.0)	262.4	(472.3)	184.2	(331.5)	123.2	(221.8)	263.5	(474.3)

* As measured from hydrogen inlet (see fig. 1).
** Throat location
*** Wall Temperatures correspond to point midway between stated and preceding axial location.

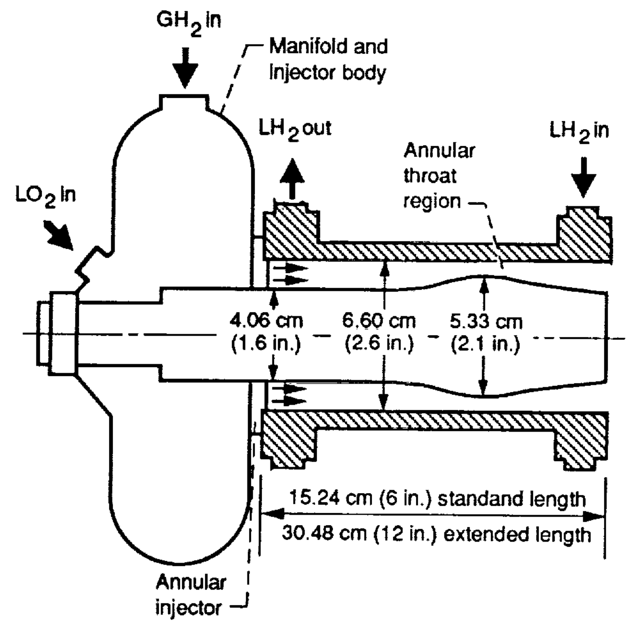

Figure 1.—Schematic of cylindrical thrust chamber assembly.

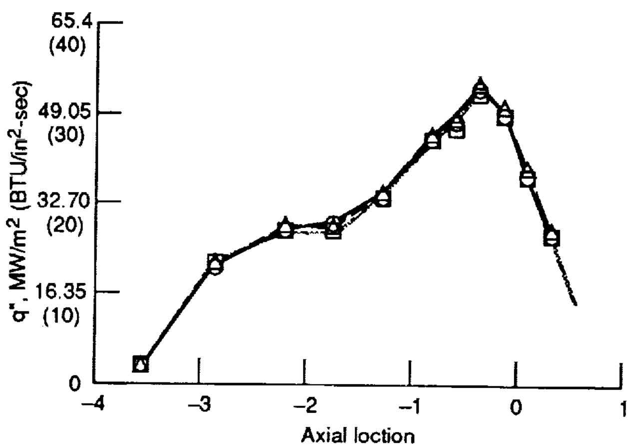

Figure 3.—Heat flux vs. axial location.

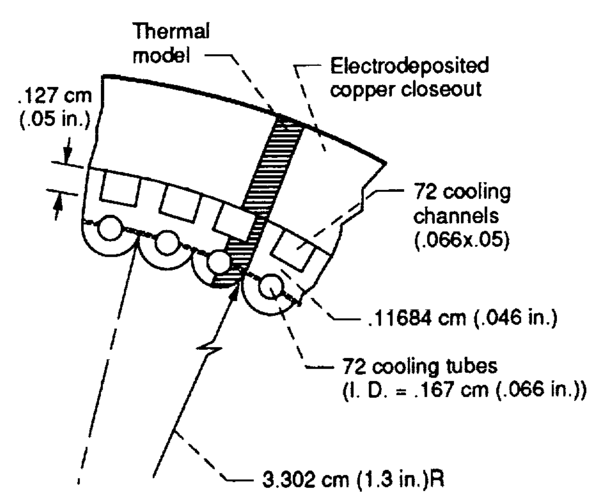

Figure 2.—Cylinder wall cross section showing geometry.

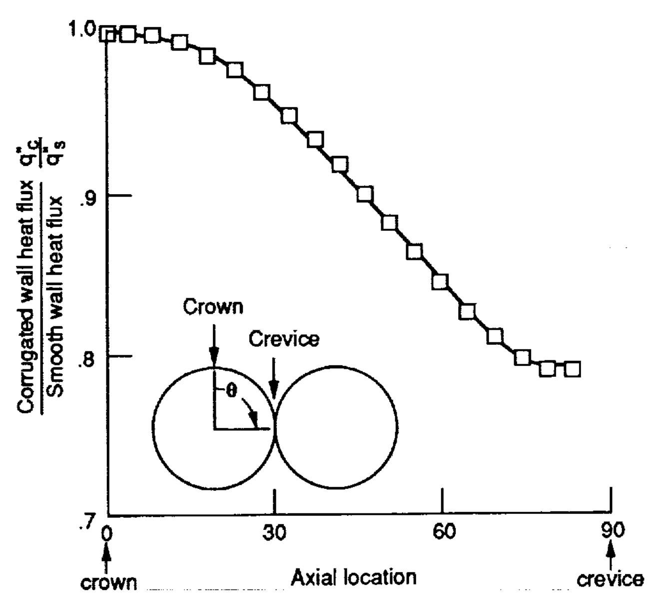

Figure 4.—Heat flux comparison between smooth and corrugated wall rocket engines.

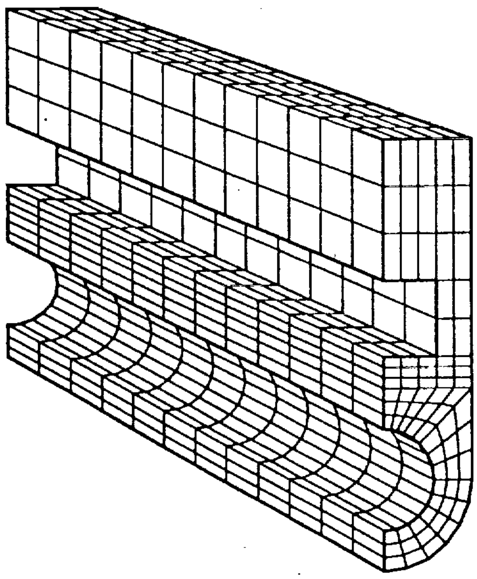

Figure 5.—Three dimensional model, 912 nodes.

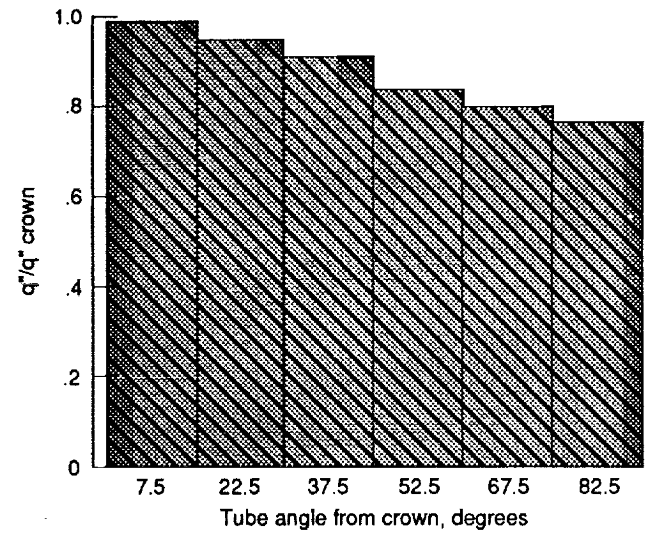

Figure 7.—Circumferential variation of heat flux applied to dual cooled analysis.

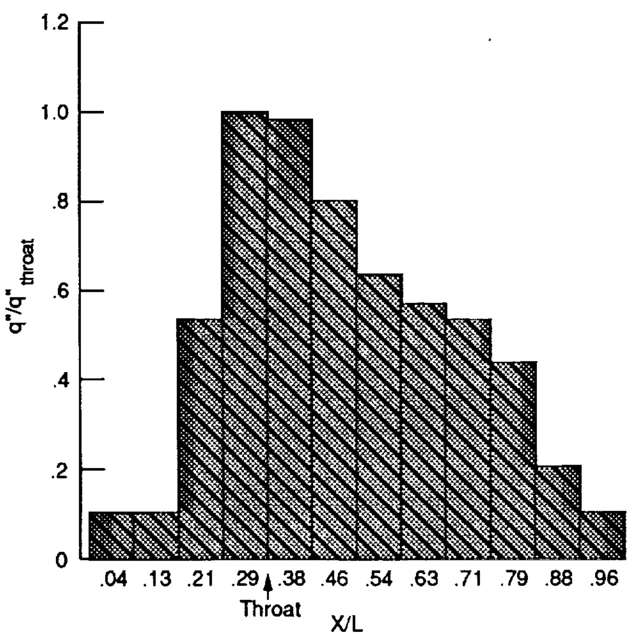

Figure 6.—Axial variation of heat flux applied to dual cooled analysis.

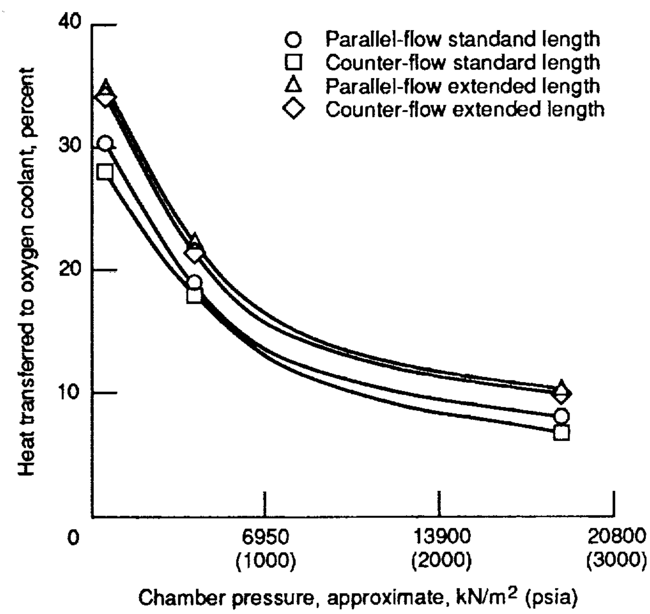

Figure 8.—Global heat transfer ability of oxygen coolant.

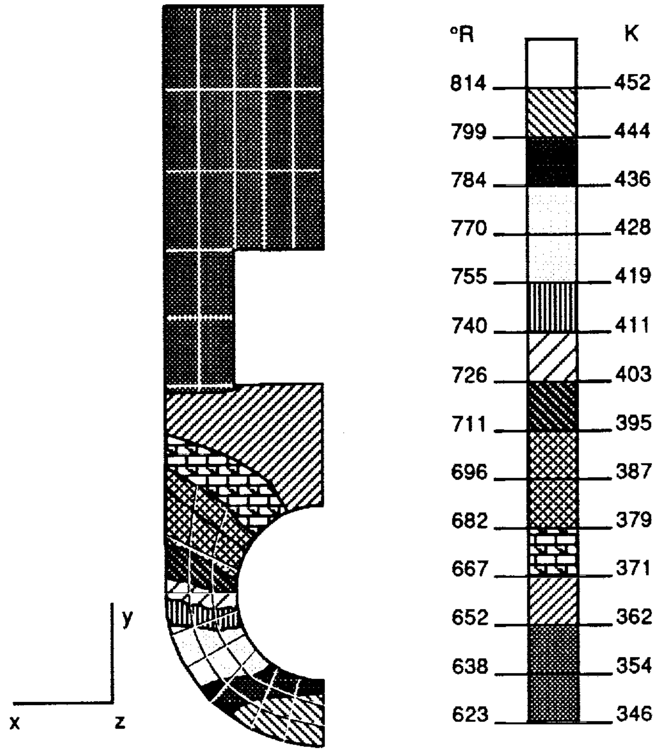

(a) Low coolant flow/low heat flux.

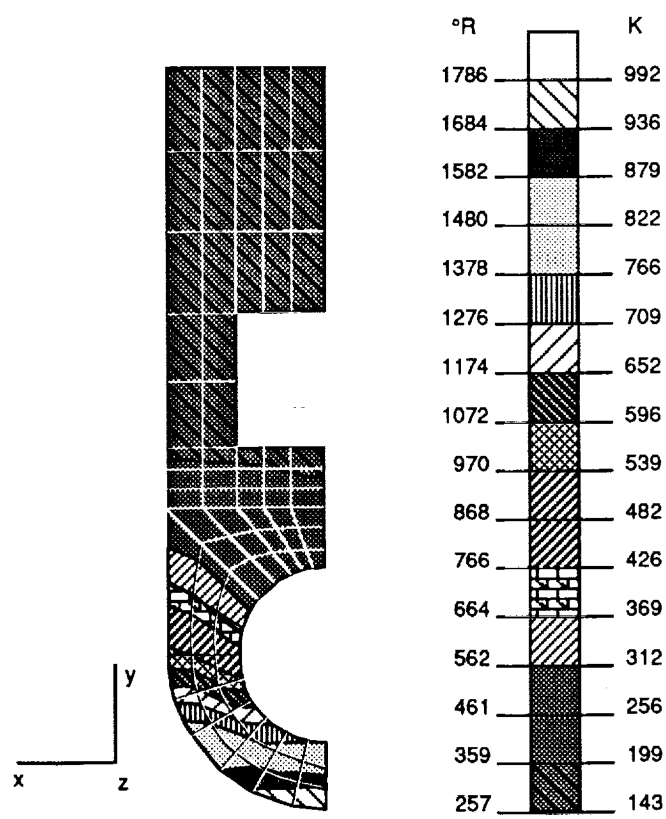

(b) High coolant flow/high heat flux.

Figure 9.—Throat temperature distributions of dual-cooled spoolpiece.

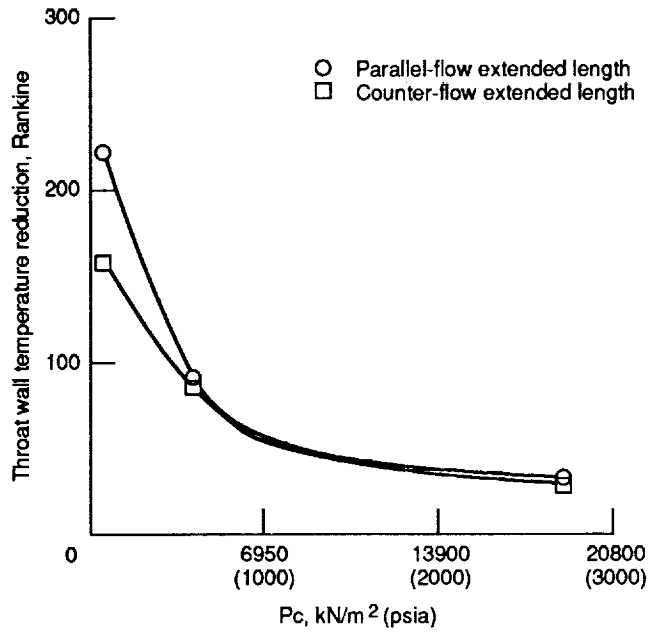

Figure 10.—Reduction in hot side wall throat temperature possible with dual cooling.

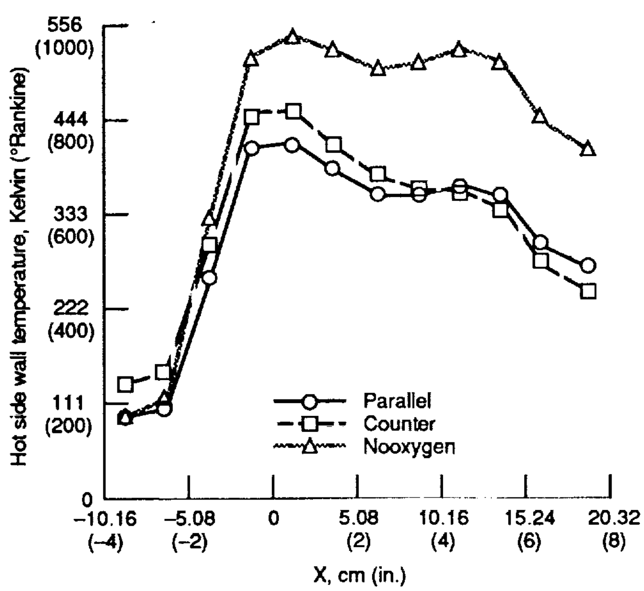

Figure 11.—Hot side wall temperature of extended length throttled spoolpiece.

NASA
National Aeronautics and Space Administration

Report Documentation Page

1. Report No. NASA TM-104430 AIAA-91-2211	2. Government Accession No.	3. Recipient's Catalog No.
4. Title and Subtitle A Dual-Cooled Hydrogen-Oxygen Rocket Engine Heat Transfer Analysis		5. Report Date
		6. Performing Organization Code
7. Author(s) Kenneth J. Kacynski, John M. Kozaroff, and Robert S. Jankovsky		8. Performing Organization Report No. E-6186
		10. Work Unit No. 593-12-21
9. Performing Organization Name and Address National Aeronautics and Space Administration Lewis Research Center Cleveland, Ohio 44135-3191		11. Contract or Grant No.
		13. Type of Report and Period Covered Technical Memorandum
12. Sponsoring Agency Name and Address National Aeronautics and Space Administration Washington, D.C. 20546-0001		14. Sponsoring Agency Code

15. Supplementary Notes

Prepared for the 27th Joint Propulsion Conference, cosponsored by the AIAA, SAE, ASME, and ASEE, Sacramento, California, June 24-26, 1991. Responsible person, Kenneth J. Kacynski, (216) 433-2469.

16. Abstract

This report describes the potential benefits of simultaneously using hydrogen and oxygen as rocket engine coolants. A plug-and-spool rocket engine (15.24 and 30.28 cm (6 and 12 in.) long) was examined at heat fluxes ranging from 9290 (5.68) to 163 500 (100) kW/m^2 (Btu/in.^{2}-sec), using a combined (i.e., "tied") three-dimensional conduction/advection analysis. Both counter flow and parallel flow cooling arrangements were analyzed. The results indicate that a significant amount of heat transfer to the oxygen will occur, thereby, reducing both the hot side wall temperature of the rocket engine and also reducing the exit temperature of the hydrogen coolant. In all heat flux and coolant flow rates examined, the total amount of heat transferred to the oxygen was found to be largely independent of the oxygen coolant flow direction. At low heat flux/low coolant flow (i.e., throttled) conditions, the oxygen coolant absorbed more than 30 percent of the overall heat transfer from the rocket engine exhaust gasses. Also, hot side wall temperatures were judged to decrease by approximately 200° in the throat area and up to a 400° combustion chamber wall temperature reduction is expected if dual cooling is applied. The reduction in combustion chamber wall temperatures at throttled conditions is especially desirable since the analysis indicates that a double temperature maxima, one at the throat and another in the combustion chamber, will occur with a traditional hydrogen cooled only engine. Conversely, a dual cooled engine essentially eliminates any concern for overheating in the combustion chamber.

17. Key Words (Suggested by Author(s)) Hydrogen oxygen engines; Combustion chamber; Heat exchanger; Throttling; Dual cooled	18. Distribution Statement Unclassified - Unlimited Subject Category 20

19. Security Classif. (of the report)	20. Security Classif. (of this page)	21. No. of pages	22. Price*
Unclassified	Unclassified	16	A03

NASA FORM 1626 OCT 86

*For sale by the National Technical Information Service, Springfield, Virginia 22161